Highly Mesoporous Carbon Aerogel as Catalyst Support in Proton Exchange Membrane Fuel Cells

By Eric Kim and Kevin Gu

Category: Energy: Sustainable Materials & Design

I. ABSTRACT

Carbon aerogel possesses unique structural and electrical properties, such as high mesopore volume, specific surface area, and electrical conductivity, which make it suitable for use as a catalyst support in Proton Exchange Membrane Fuel Cells (PEMFC). In this study, we present a novel synthesis of highly mesoporous carbon aerogel via ambient-drying and its application in PEMFCs. The structural effects of activation on carbon aerogel were also studied. Nitrogen adsorption-desorption, Non Localized Density Function Theory (NLDFT) analysis were carried out to observe the morphology and pore characteristics. We find that a resorcinol/catalyst ratio of 200 yields carbon aerogel with the highest mesopore ratio and volume. Pt on carbon aerogel and activated carbon aerogel show efficient activity in both oxygen reduction and hydrogen oxidation reactions compared to Pt on Vulcan XC-72, with increases up to 715% and 195% in specific power density, respectively. The enhanced performance of carbon aerogel is attributed to its high mesopore volume and low micropore volume. Activation increases total pore volume but also increases micropore volume, which limits oxygen transport at the cathode. Accelerated stress tests show that carbon aerogel has comparable durability with Vulcan XC-72, while activated carbon aerogel is less durable than both materials. Thus, the mesoporous carbon aerogel provides an efficient, lower-cost alternative to existing microporous carbon material as a catalyst support in PEMFCs.

Keywords: Carbon aerogel, activation, fuel cells, mesoporous

II. INTRODUCTION

Proton exchange membrane fuel cells (PEMFC) have recently seen interest as a prospective new energy conversion system [1]. The development of alternative energy sources has been of focus to decrease the emission of greenhouse gases from the burning of fossil fuels [2-4]. The fuel cell's applications are diverse, ranging from transport, stationery, medical, and more [5-6]. PEMFCs can be utilized as efficient chemical converters especially in transport vehicles, which is largely attributed to their high efficiency, high power density, and low operating temperature [7-10]. The cell's primary component is the MEA, which includes a membrane and electrodes, which facilitates the chemical process of the oxygen reduction reaction (ORR) and the hydrogen oxidation reaction (HOR) [11-12]. Some challenges need to be addressed to further enhance the fuel cell's potential in the scientific community, though, including its lower durability and higher cost compared to their combustion engine counterparts [13-15]. One method of mitigating these issues is to utilize supported catalysts with lower noble metal loadings.

Carbon materials possess unique structural and electrical properties which make it suitable for use as a catalyst support in PEMFC [16-18]. A high mesopore volume is desirable in catalyst support to ensure contact between the catalyst metal and the electrolyte [19-21]. A number of carbon supports have been investigated, such as carbon black, carbon nanotubes, graphenes, and carbon aerogels [22-27]. Carbon black, in particular, is a widely used catalyst support due to its cheap cost of production and wide availability. However, its high micropore volume, disorganized mechanical structure, and low conductivity all contribute to poor performance in PEMFC by limiting the diffusion of reactants and products [28-32]. Thus, carbon black does not make efficient use of the precious metal catalyst and negates its cheaper price. Carbon nanotubes and graphenes have better electrical conductivity but are not suitable for commercialization due to their high manufacturing costs [33-35]. Difficulty in platinum

impregnation has also been observed in these materials [36-38]. Carbon aerogels have been proposed as efficient catalyst supports due to its high electrical conductivity, high surface area, and tunable mechanical structure.

Synthesis of carbon aerogel has four major steps: gelation, aging, drying, and carbonization. The conventional drying method utilizes supercritical fluid drying to maintain the pore structure and mesoporosity while removing the solvent. However, supercritical drying requires the use of several expensive components which drives up the cost of production. Alternative drying methods have been observed such as freeze-drying and template-based method. Yet, these methods involve numerous chemical processing techniques and result in high density, microporous carbon aerogels. Furthermore, previous research has shown that these methods also yield low electrochemically active surface areas, resulting in low support conductivity.

Activated carbon aerogel based catalysts are novel methods used in applications in hydrogen fuel cells. Several papers have documented its use in supercapacitors and microbial fuel cells. However, the microporous properties of the activated carbon aerogels make them unsuitable for use in PEMFC. A new synthesis method was thus engineered in this paper to help further increase mesopore volume and surface area, two parameters deemed significant for PEMFC catalyst improvement supported by previous research. In this research, an efficient yet inexpensive synthesis method of carbon aerogel and activated carbon aerogel was devised using ambient drying to reduce the costs as an alternative to the traditional supercritical-drying process.

This paper presents a novel, cost-effective synthesis method of mesoporous carbon aerogels as catalyst supports for platinum in PEMFC. Carbon aerogels was produced via sol-gel polymerization of resorcinol and formaldehyde and solvent exchange with DI water. The gels were subsequently dried ambiently and carbonized under N_2 flow. The activated carbon aerogel was further treated in a CO_2 atmosphere to increase pore volume and surface area [39-42]. This synthesis process is a facile, cost-effective approach to manufacturing carbon aerogels. Platinum impregnation was based on the traditional metal precursor and sodium borohydride reduction method [43].

Barrett-Joyner-Halenda (BJH) and Non-Localized Density Functional Theory (NLDFT) was used to characterize the porosity and pore size distribution of the carbon materials. Accelerated stress tests are also conducted to compare the durability of catalyst support [44]. This research develops, synthesizes, and characterizes carbon aerogel supported catalysts with various pore size distributions, surface areas, and electrocatalytic activities in comparison with the commercial platinum on carbon black catalyst with the same loading.

III. EXPERIMENTAL

The carbon aerogel was synthesized through a process of sol-gel polymerization, solvent exchange, ambient-drying, and carbonization, as shown in Figure 1. The aerogel was further activated to yield activated carbon aerogel.

A. SYNTHESIS OF ORGANIC AEROGEL

3.08 g of resorcinol (R) and 0.016 g of sodium carbonate (C) were dissolved in 50.4 mL of water (W). The mixture was magnetically stirred for 20 minutes. 0.51 mL of 37% wt formaldehyde solution (F) was added to the mixture and stirred for an additional 5 minutes. The mixture was heated in a sealed

container at 50 °C for 24 h and 85 °C for 48 h. The R-F gel was washed with excess amounts of acetone, solvent exchanging every 24 h. The gel was then dried in a vacuum oven at 100 °C.

B. CARBONIZATION & ACTIVATION

The organic gel was carbonized and activated in a Lindberg Blue M Tube Furnace. Equal amounts of organic R-F aerogel were loaded into two ceramic boats. Both boats were carbonized under an N_2 atmosphere at 800 °C for 2 h at a heating ramp of 10 °C/min. After pyrolysis, the furnace was allowed to cool to 300 °C. One boat was taken out to cool to room temperature and the other was activated under CO_2 atmosphere at 900 °C for 2 h at a heating ramp of 10 °C/min.

C. IMPREGNATION

The carbon was ground to obtain a fine powder. 100 mg of carbon powder was dispersed into 80 mL of DI water. The mixture was then stirred for 20 minutes and further sonicated for another 20 minutes. 2.6 mL of 0.1 M H_2PtCl_6 was added to the solution drop by drop under continuous magnetic stirring. The mixture was sonicated for 20 minutes. A stoichiometric excess of 0.6 M $NaBH_4$ was dispersed drop-wise as the reducing agent and sonicated for 1 h. The solution was finally filtered using a Buüchner funnel and washed several times with DI water. Desired Pt powder was obtained after heating at 80 °C overnight.

D. MEA PREPARATION

50 mg of catalyst powder was mixed with 222 mg of 15% Nafion solution, 0.53 mL of DI water, and 2.5 mL of IPA. The solution was thoroughly mixed overnight to form the catalyst ink. The ink was applied onto the 5 cm^2 papers of Sigracet 29 BC carbon paper using a spray gun. The papers were placed onto a heating plate to keep the surface temperature of the paper at 85 °C to evaporate the excess liquid. Finally, electrodes with the desired Pt loading of 0.1 mg/cm^2 (40 wt%) were obtained for both cathode and anode sides. The membrane electrode assembly (MEA) was prepared by putting the current collector, electrodes, and a 5 cm^2 Nafion 117 membrane together.

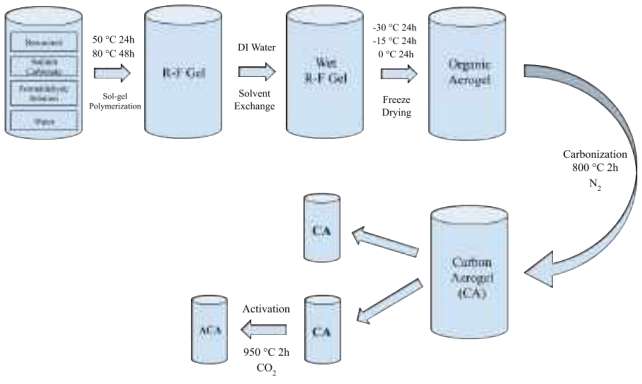

Scheme 1. Synthesis of Carbon Aerogel/Activated Carbon Aerogel.

IV. RESULTS AND DISCUSSION

CHARACTERIZATION

Nitrogen adsorption and desorption measurements were carried out with the NOVAtouch LX^2. The desorption branch for carbon black (CB) was used for the Barrett-Joyner-Halenda (BJH) calculation. Given the fact that Vulcan XC-72 was mostly microporous in composition, BJH modeling gave an accurate pore size distribution. Non-Localized Density Functional Theory (NLDFT) was used to model the pore distribution and surface area for carbon aerogel (CA) and activated carbon aerogel (ACA). NLDFT gives a more accurate analysis of mesoporous materials by filling in the gap at the 10 nm pore size range in BJH modeling.

EDXRF elemental analysis was conducted using a Rigaku NEX DE. The analysis was conducted in a helium atmosphere. TEM imaging was conducted using a JEOL JEM 1400 Transmission Electron Microscope. Images were obtained at 50x and 100x magnification.

The prepared MEA was tested in a fuel cell test station from Fuel Cell Technologies, Inc. Electrochemical tests were conducted in four different environments: 60 °C H_2/air, 60 °C H_2/O_2, 80 °C H_2/air, and 80 °C H_2/O_2.

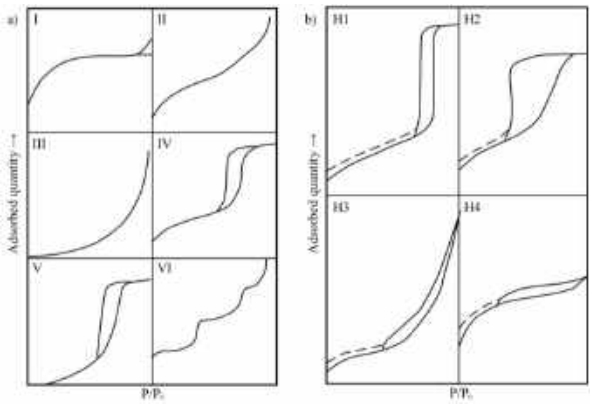

Figure 1. (a) 6 Types of isotherms; **(b)** 4 types of hysteresis loops.

A. NITROGEN ADSORPTION ISOTHERMS

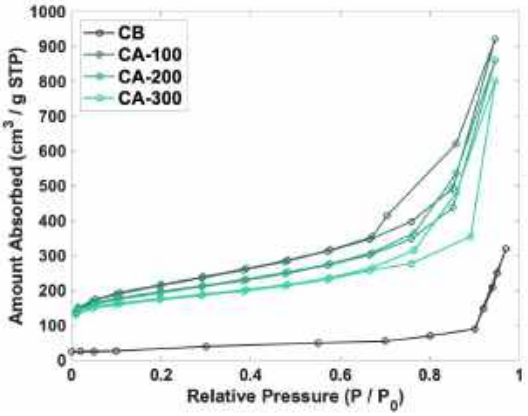

Figure 2. Adsorption isotherms of nitrogen on CB, CA-100, CA-200, CA-300 at 77 K.

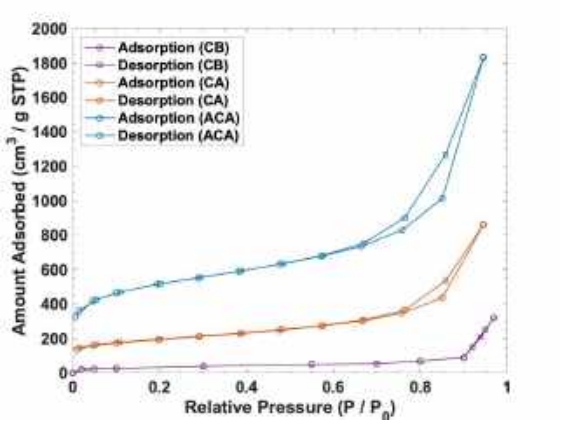

Figure 3. Adsorption isotherms of nitrogen on CB, CA, and ACA at 77 K.

The adsorption isotherms of nitrogen on CB, CA-100, CA-200, and CA-300 are shown in Figure 2. The adsorption isotherms of nitrogen on CB, CA, and ACA are shown in Figure 3. The isotherms can be characterized by the IUPAC classification, shown in Figures 1a and 1b.

The adsorption isotherms of CB is type I. Type I isotherms are categorized as microporous materials with small external surfaces, such as activated carbons, molecular sieve zeolites, or porous oxides, with the limiting uptake controlled by the accessible micropore volume instead of the internal surface area.

The adsorption isotherms of CA and ACA are both of type IV and have a clear hysteresis. Type IV isotherms are characterized by their hysteresis loops, which are correlated with the capillary condensations within mesopores, and the limiting uptake over a range of high p/p0. The initial curve of the isotherm can be largely accredited to the monolayer-multilayer adsorption as it accompanies the same path as that of the Type II isotherm from the given adsorptive on the same surface area in a nonporous form. Many industrial adsorbents give Type IV isotherms.

The hysteresis of CA and ACA are of type H3. The shape of the hysteresis loop is indicative of the type of pores present. Type H3 loops do not demonstrate limiting adsorptions at high p/p0 and are observed with aggregates of plate-like particles, exhibiting slit-shaped pores.

B. SURFACE AREA & PORE VOLUME

Table 1 shows the total pore volume, micropore and mesopore pore volume and the mesopore % for CA synthesized with R/C ratio 100, 200, and 300. Table 2 shows the surface area and pore volume analysis for CB, CA, and ACA. It can be seen that two hours of activation on CA increases the surface area by 150% and increases both micropore and mesopore volume by 194% and 103% respectively. It is also observed that CB and CA has comparable micropore volume. However, CA and ACA show an increase of 444 and 802 times in mesopore volume in comparison with carbon black, respectively.

Material	V_{total} (cm^3/g)	V_{micro} (cm^3/g)	V_{meso} (cm^3/g)	Mesopore %
Vulcan XC-72	0.1823	0.1790	0.0033	1.81
CA-100	1.012	0.19	0.82	81.0
CA-200	1.314	0.17	1.14	86.8
CA-300	1.20	0.17	1.03	84.4

Table 1. R/C Ratio Analysis

Material	S_{total} (m^2/g)	S_{micro} (m^2/g)	S_{meso} (m^2/g)	V_{total} (cm^3/g)	V_{micro} (cm^3/g)	V_{meso} (cm^3/g)
CB	266	262.4	3.6	0.1823	0.1790	0.0033
CA	643	407	236	1.314	0.17	1.14
ACA	1600	1102	498	2.823	0.5	2.32

Table 2. Surface Area and Pore Volume.

C. PORE ANALYSIS

Figures 4, 5, and 6 show the pore size distribution curves of CB, CA, and ACA derived from the adsorption branches of the isotherms using the BJH and NLDFT method. The pore size distribution of carbon black is very narrow and drops to near zero above 2 nm compared to the two aerogels. The results reveal that the material is microporous, and have little to no mesopores. PSD of carbon black peak at 1.30 nm, and the average pore diameter is 1.35 nm. On the other hand, the aerogels have a much broader size distribution with pore diameters up to 40 nm. The results reveal that both aerogels contain many micropores and mesopores. PSD of CA show peaks at 0.73 nm and 10.6 nm, while PSD of ACA shows peaks at 0.8 nm and 10.2 nm. The average pore size for CA and ACA is 9.1618 nm and 8.6454 nm respectively.

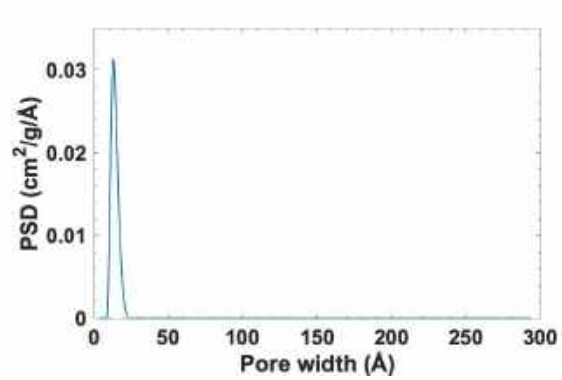

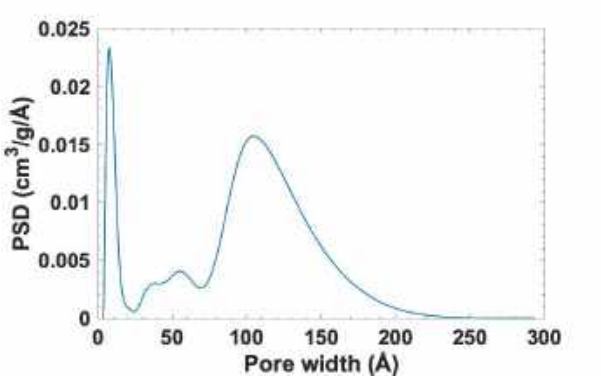

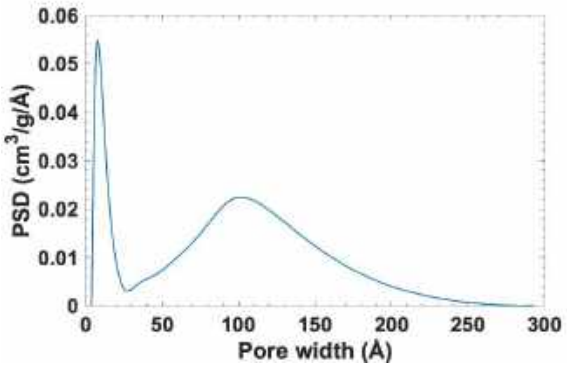

Figure 4. CB pore distribution. **Figure 5.** CA pore distribution **Figure 6.** ACA pore distribution.

CATALYST POWDER ANALYSIS

A. X-RAY FLUORESCENCE

Figure 7 shows the different EDXRF spectrums of Pt/CB, Pt/CA, and Pt/ACA. Despite contamination, all graphs show a peak at 9.442 keV, indicating the presence of platinum particles in the catalyst powder. The XRF data confirms that the impregnation process through $NaBH_4$ reduction was successful. Comparing the relative peaks for Pt-Lα, it can be concluded that all three catalyst powders have similar platinum contents. However, due to its non-homogenous property and high carbon content, an accurate weight percentage of platinum cannot be obtained.

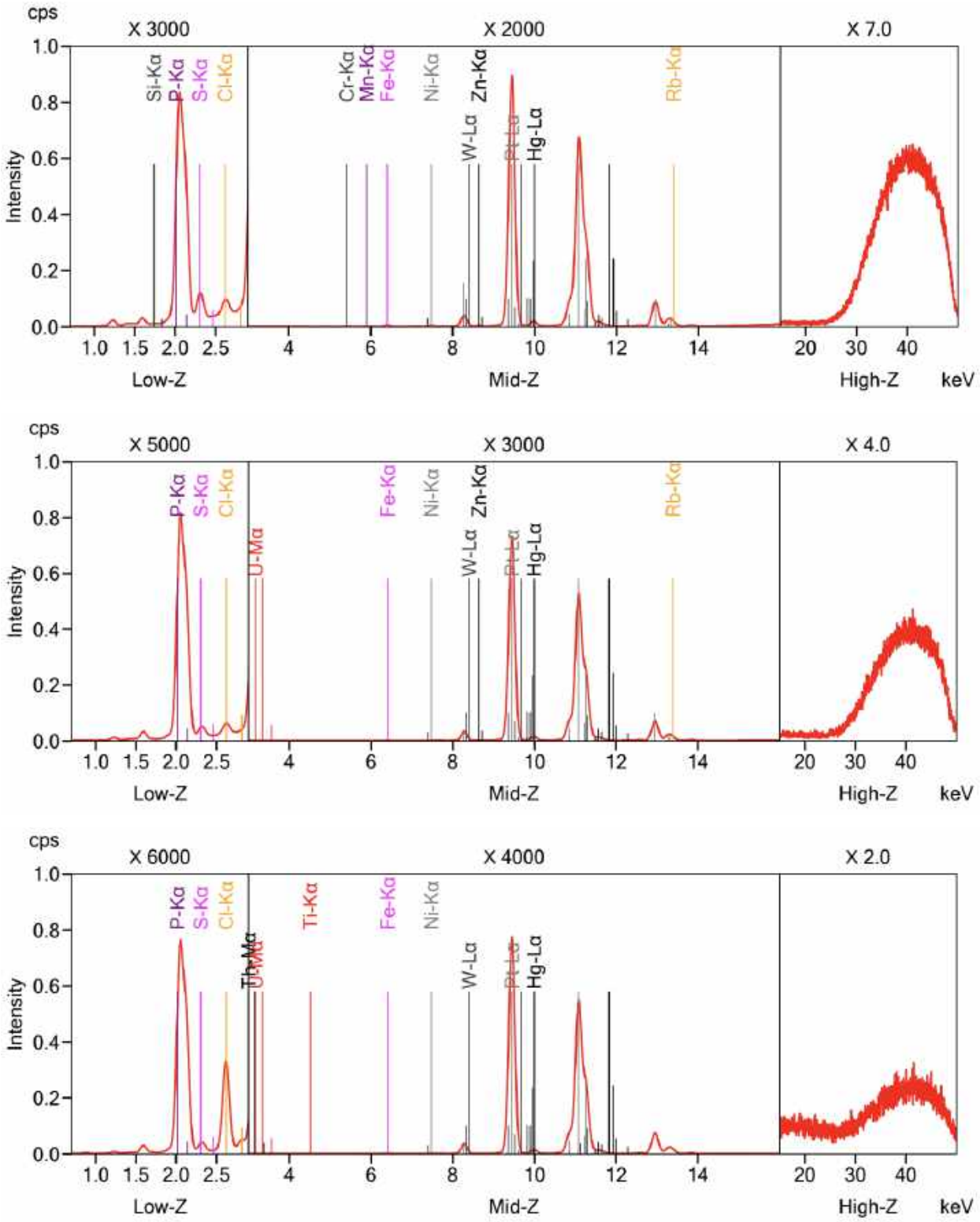

Figure 7. Graph of EDXRF Spectrums for Pt/CB, Pt/CA, and Pt/ACA.

B. TRANSMISSION ELECTRON SPECTROSCOPY

TEM imaging was conducted using a JEOL JEM 1400 Transmission Electron Microscope on platinum on CB (Pt/CB), platinum on CA (Pt/CA), platinum on CB (Pt/CB). Images were obtained at 50x and 100x magnification.

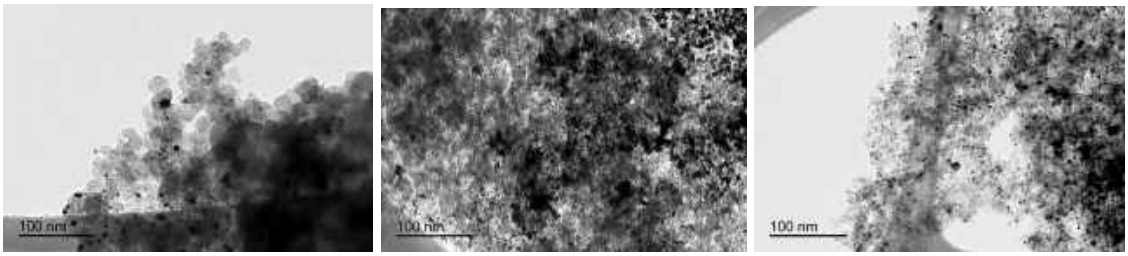

Figure 8. TEM of Pt/CB, Pt/CA, and Pt/ACA catalyst powder at 50x magnification.

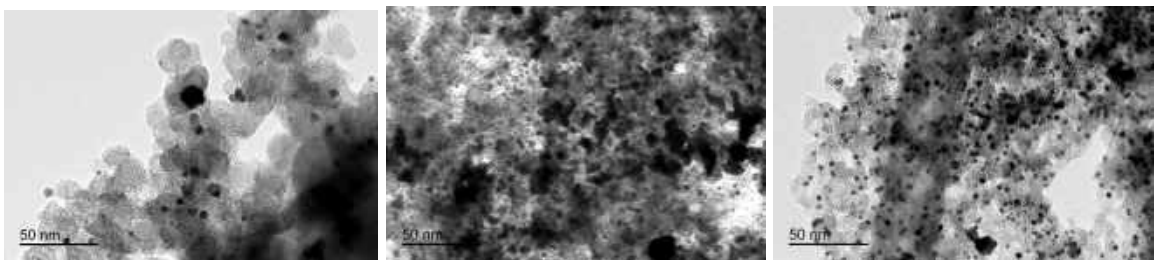

Figure 9. TEM of Pt/CB, Pt/CA, and Pt/ACA catalyst powder at 100x magnification.

The TEM imaging for Pt/CB, Pt/CA, and Pt/ACA at 50x and 100x magnification are shown in Figures 8 and 9, respectively. The particles are shown to form large aggregates in the Pt/CB (50 nm). The larger aggregates with more dispersed Pt particles are likely to corrode faster. Agglomeration leads to the inhibition of transport and formation of product in the anode of the fuel cell, which leads to use of carbon and water as reactant. This mechanism causes detonation of catalyst and results in poor performance in the cell. In contrast, the Pt particles on Pt/CA and Pt/ACA are evenly distributed and are similar in size.

Average particle size of the platinum on Pt/CB, Pt/CA, and Pt/ACA obtained from the TEM imaging are 3.853, 2.517, and 3.15 nm, respectively. The overall electrochemically active surface area (ECSA) of platinum particles in the catalyst layer can be estimated using the equation $S = \frac{6 * m}{p * d}$, where m and p are the mass and density of platinum and d is the average particle size. According to the equation, average particle size is inversely proportional to the ECSA [45]. Therefore, the ECSA of the three powders can be ordered as Pt/CA, Pt/ACA, Pt/CB, in decreasing order. The higher ECSA of Pt/CA suggests that it will have the highest performance in the fuel cell, as ECSA is directly correlated with power output. The standard deviation of Pt particles on Pt/CB, Pt/CA and Pt/ACA are 1.425, 0.8545, and 0.6982, respectively. TEM imaging illustrates the superior qualities of uniform particle size and dispersion of Pt particles on Pt/CA and Pt/ACA in comparison to Pt/CB.

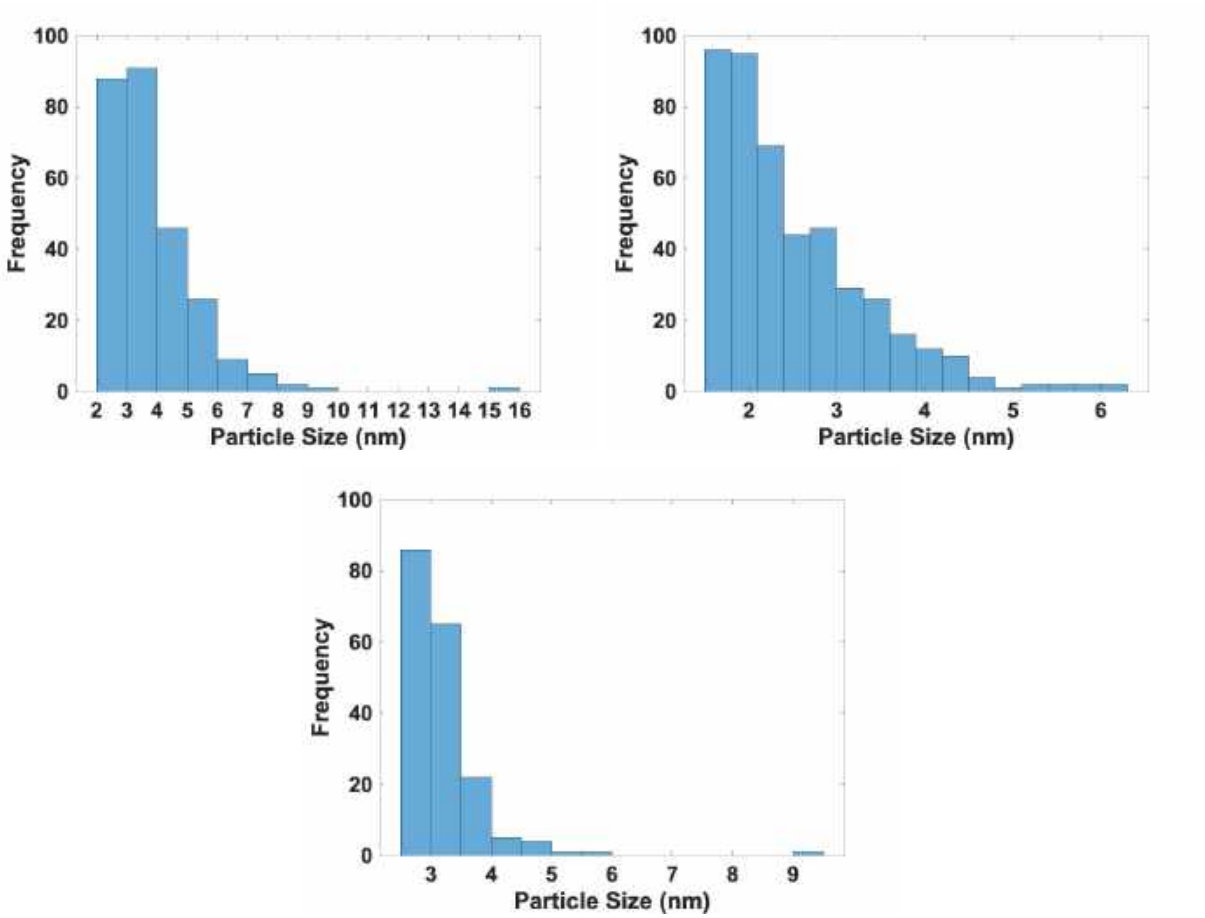

Figure 10. Histograms of particle size distribution of Pt/CB, Pt/CA, Pt/ACA.

ELECTROCHEMICAL PERFORMANCE

A. FUEL CELL TEST

The fuel cell performances of Pt/CB, Pt/CA, and Pt/ACA in testing environments of 60 °C H2/air, 60 °C H2/O2, 80 °C H2/air, and 80 °C H2/O2 are shown in table 2 and figures 11, 12, 13 and 14, respectively.

In a typical voltage-current density curve, a rapid decrease of voltage illustrates the effect of mass transport drops. In the four environment conditions, it can be observed that Pt/CB exhibits a relatively more negative slope in comparison to Pt/CA and Pt/ACA, indicating a blocking of mass transport. These can be attributed to its high micropore volume and agglomeration in the catalyst, as shown in Figure 8. The Pt/CA shows a relatively small decrease of cell voltage, indicating superior mass transport mechanisms which are supported by its high surface area and organized mechanical structure. Pt/ACA shows subpar performance, which can be attributed to its high micropore volume. The high micropore volume creates a bottleneck at the surface of Pt/ACA, hence rendering the inner surface area unusable for platinum deposition.

Comparing the peak power densities of all three materials at different conditions, Pt/CA shows the greatest power density, followed by Pt/ACA, and lastly Pt/CB. In comparison with Pt/CB at 60 °C in H_2 / Air, Pt/CA and Pt/ACA have an increase in density at 644% and 36%, respectively. For 60 °C in an H_2 / O_2 atmosphere, Pt/CA has an increase of 613% while Pt/ACA has an increase of 155%. In 80 °C H_2 /

Air, Pt/CA increases 87% and Pt/ACA increases 45%. For 80 °C H_2 / O_2, Pt/CA exhibits a 715% increment and Pt/ACA a 195% increase.

B. DURABILITY TEST

A standard accelerated stress test (AST) was conducted on all the MEAs for 10,000 cycles to assess the durability of the MEA. The AST protocol is performed in H_2 atmosphere for the anode and N_2 atmosphere for the cathode at 80 °C. The protocol consists in jumping between two potentials, 2 seconds at 0.6 V and 2 seconds at 0.96 V.

The voltage at 100 mA/cm^2 before and after the AST, and the loss in voltage per cycle is shown in Figure 15. Pt/CA showed a significant increase in voltage after 10,000 cycles in 80 °C H_2 / Air while other materials showed a decrease in voltage. For all other environments, Pt/CB and Pt/CA showed comparable durability while Pt/ACA showed slightly worse durability.

Material	60_{Air} (mW)	60_{Oxy} (mW)	80_{Air} (mW)	80_{Oxy} (mW)
Pt/CB	223.9	412.0	270.0	393.3
Pt/CA	1667	2938.4	505.6	3210.5
Pt/ACA	306.5	1052.3	391.8	1160

Table 2. Peak power for Pt/CB, Pt/CA, and Pt/ACA at different conditions.

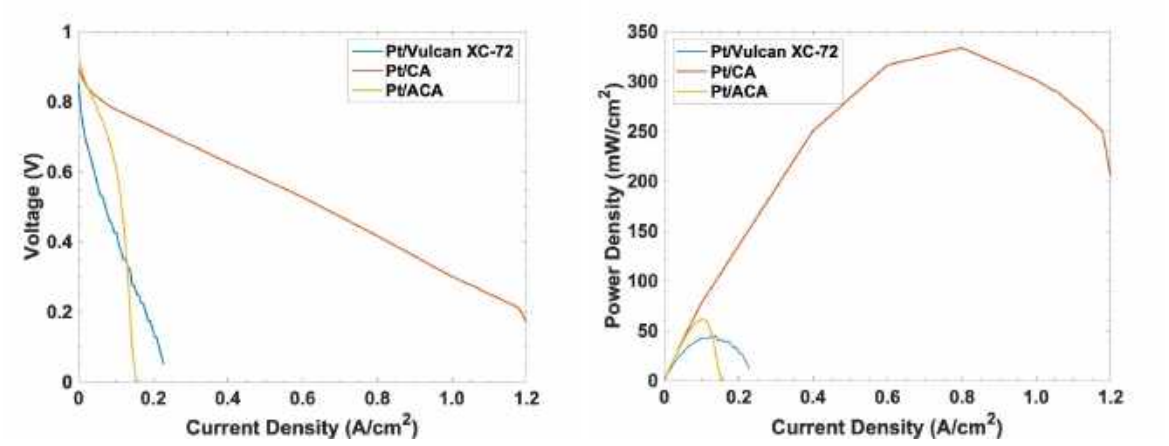

Figure 11. Fuel Cell Performance at 60 °C in H_2 / Air.

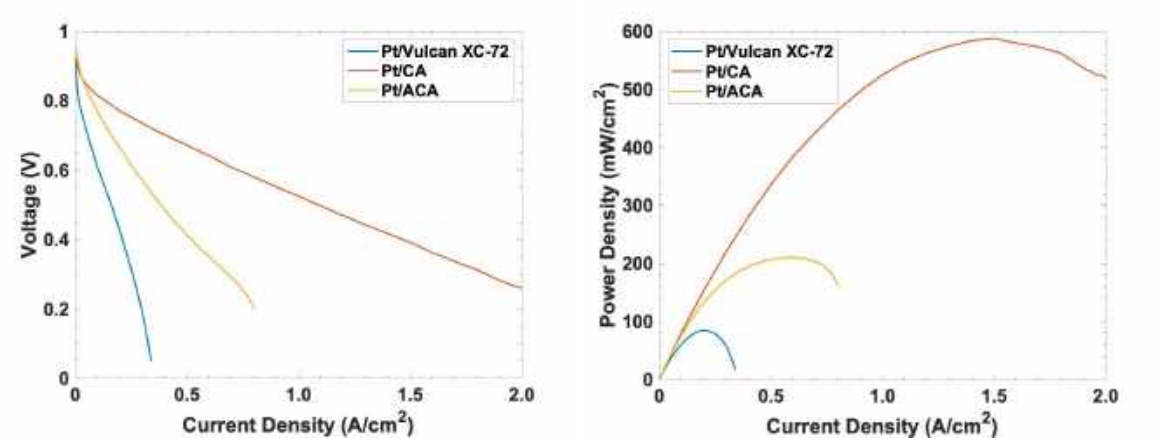

Figure 12. Fuel Cell Performance at 60 °C in H_2 / O_2.

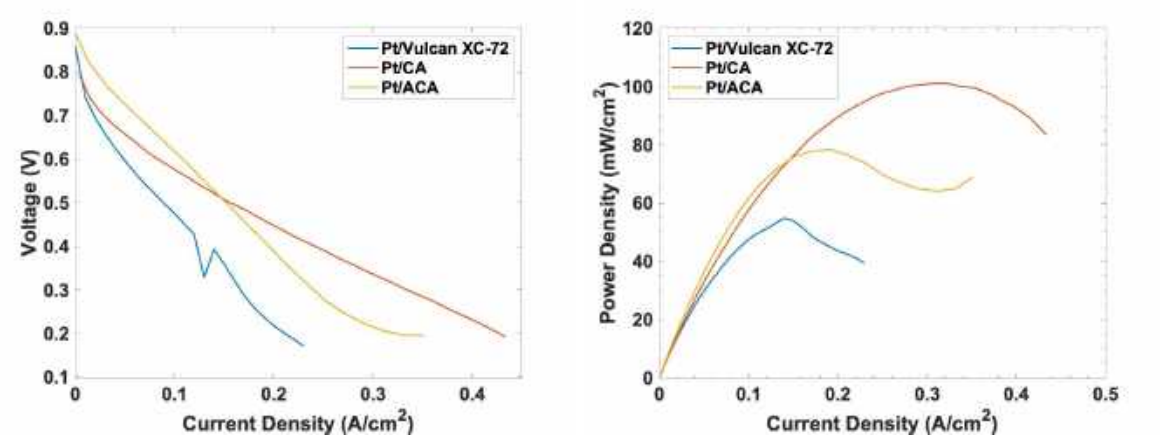

Figure 13. Fuel Cell Performance at 80 °C in H_2 / Air.

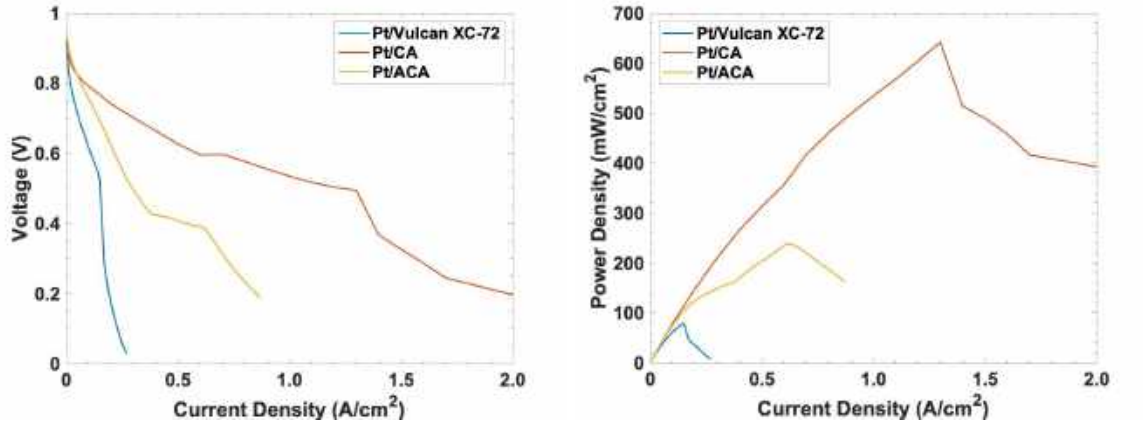

Figure 14. Fuel Cell Performance at 80 °C in H_2 / O_2.

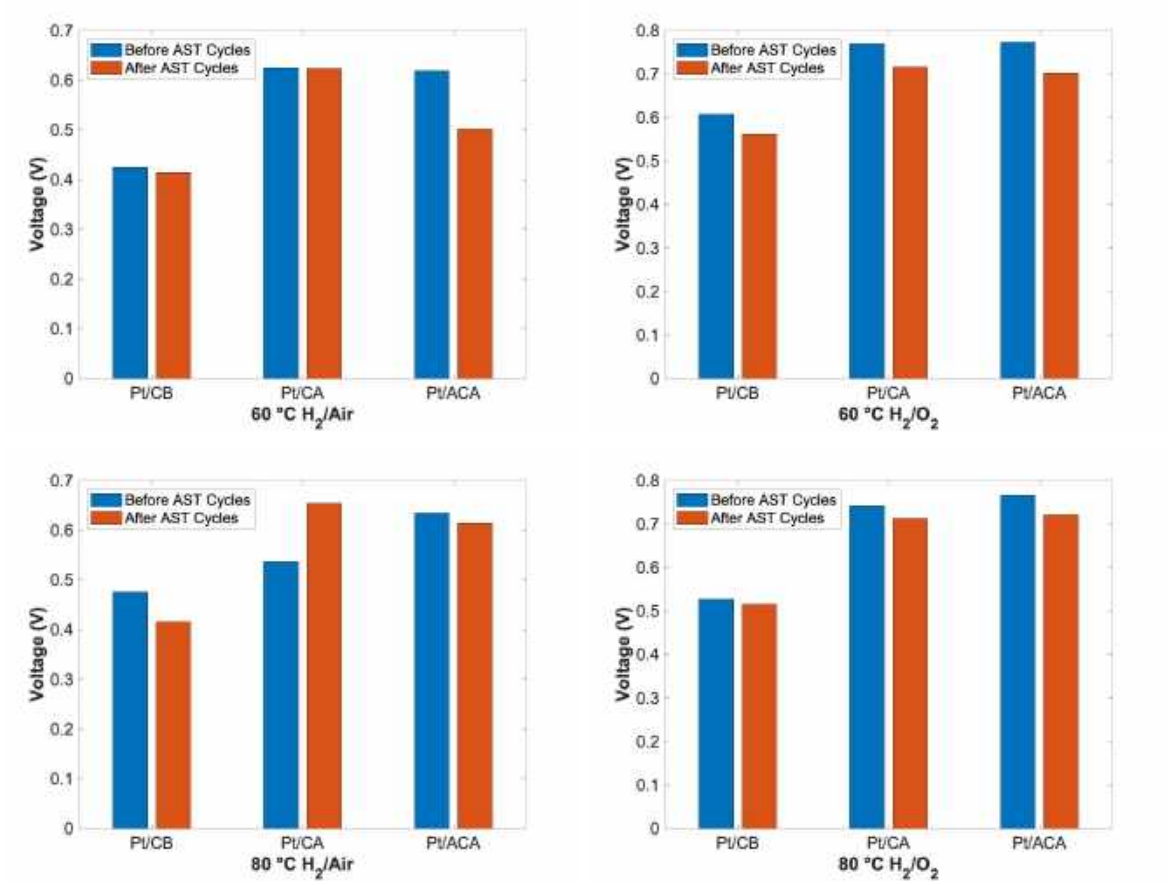

Figure 15. Voltage at 100 mA/cm^2, for Pt/CB, Pt/CA, and Pt/ACA, before and after 10,000 AST durability cycles at different conditions.

VIII. CONCLUSION

We have demonstrated a low-cost synthesis of carbon aerogel and activated carbon aerogel and its application in a PEMFC. A highly mesoporous carbon aerogel with a surface area of 643 m^2/g and mesopore volume of 1.14 cm^3/g is produced. Activation of this carbon aerogel in CO_2 atmosphere for two hours at 950 °C degrees outputs activated carbon aerogel with a high surface area of 1600 cm^2/g and mesopore volume of 2.32 cm^3/g.

Both electrochemical characterizations of Pt/CA and Pt/ACA indicate the efficient activity in both ORR and HOR reactions relative to that of Pt/CB. These results can likely be attributed to higher mesopore to micropore ratio, and even distribution of catalyst particles. High micropore volume in CB and ACA, however, creates a nucleation site for Pt deposition, which negatively affect the performance. The fuel cell performance after 10,000 cycles is used to assess the durability of the materials, in which carbon aerogel shows comparable durability with Vulcan XC-72, while activated carbon aerogel is less durable than both materials.

The results find that high mesopore volume and low micropore volume suggests high efficiency. Activated carbon aerogel increased surface area by 501%, but micropore volume increased by 179%, which inhibited oxygen mass transport at the cathode and decreased efficiency. Considering the

parameters measured in this research, compared to Pt/CB, Pt/CA shows an 715% increase in efficiency, further corroborating the idea that mesopore volume is indicative of PEMFC performance.

A 715% increase in peak power density by replacing carbon black with carbon aerogel indicates a great step forward in the field of hydrogen fuel cell research. A higher power output and comparable durability for Pt/CA compared to Pt/CB is a step towards decreasing costs of fuel cell manufacturing by having the potential to produce the same power output with less platinum loading. The results demonstrate that replacement of any existing microporous carbon support with high surface area, mesoporous carbon aerogel will show positive effects.

We anticipate this mesoporous carbon aerogel created from a simple procedure of sol-gel polymerization, solvent exchange, ambient-drying, and carbonization will have broad applications in the fields of supercapacitors, lithium ion batteries, and capacitive deionization.

Future work lies in testing combinations of state of the art catalysts and aforementioned mesoporous carbon aerogel. Additional CV curve and TEM image analysis on catalyst powder after durability testing can be used to observe the structural integrity of carbon aerogel and its electrochemical surface area. New methods of creating activated carbon aerogel with low micropore volume will be explored. There is also room for development in streamlining the carbon aerogel process on a larger scale for application at a commercial level.

VIII. ACKNOWLEDGEMENTS

The authors would like to thank the Garcia Center for Polymers at Engineered Interfaces at Stony Brook University for the opportunity to conduct characterization and electrochemical performance tests.

IX. CITATIONS

[1] Shimpalee, S., Lilavivat, V., Van Zee, J. W., McCrabb, H., & Lozano-Morales, A. (2011). Understanding the effect of channel tolerances on performance of PEMFCs. *International Journal of Hydrogen Energy*, 36(19), 12512–12523. https://doi.org/10.1016/j.ijhydene.2011.06.146

[2] Meinshausen, M., Meinshausen, N., Hare, W., Raper, S. C. B., Frieler, K., Knutti, R., … Allen, M. R. (2009). Greenhouse-gas emission targets for limiting global warming to 2 °C. *Nature*, 458(7242), 1158–1162. https://doi.org/10.1038/nature08017

[3] McCarthy, R., & Yang, C. (2010). Determining marginal electricity for near-term plug-in and fuel cell vehicle demands in California: Impacts on vehicle greenhouse gas emissions. *Journal of Power Sources*, 195(7), 2099–2109. https://doi.org/10.1016/j.jpowsour.2009.10.024

[4] Colella, W. G., Jacobson, M. Z., & Golden, D. M. (2005). Switching to a U.S. hydrogen fuel cell vehicle fleet: The resultant change in emissions, energy use, and greenhouse gases. *Journal of Power Sources*, 150, 150–181. https://doi.org/10.1016/j.jpowsour.2005.05.092

[5] Carrette, L., Friedrich, K. A., & Stimming, U. (2001). Fuel Cells - Fundamentals and Applications. *Fuel Cells*, 1(1), 5–39. doi:10.1002/1615-6854(200105)1:1<5::aid-fuce5>3.0.co;2-g

[6] Staffell, I., Scamman, D., Velazquez Abad, A., Balcombe, P., Dodds, P. E., Ekins, P., … Ward, K. R. (2019). The role of hydrogen and fuel cells in the global energy system. *Energy & Environmental Science*, 12(2), 463–491. https://doi.org/10.1039/C8EE01157E

[7] Peighambardoust, S. J., Rowshanzamir, S., & Amjadi, M. (2010). Review of the proton exchange membranes for fuel cell applications. *International Journal of Hydrogen Energy*, 35(17), 9349–9384. https://doi.org/10.1016/j.ijhydene.2010.05.017

[8] Rosli, R. E., Sulong, A. B., Daud, W. R. W., Zulkifley, M. A., Husaini, T., Rosli, M. I., … Haque, M. A. (2017). A review of high-temperature proton exchange membrane fuel cell (Ht-pemfc) system. *International Journal of Hydrogen Energy*, 42(14), 9293–9314. https://doi.org/10.1016/j.ijhydene.2016.06.211

[9] Staffell, I., Scamman, D., Velazquez Abad, A., Balcombe, P., Dodds, P. E., Ekins, P., … Ward, K. R. (2019). The role of hydrogen and fuel cells in the global energy system. *Energy & Environmental Science*, 12(2), 463–491. https://doi.org/10.1039/C8EE01157E

[10] Zhang, T., Wang, P., Chen, H., & Pei, P. (2018). A review of automotive proton exchange membrane fuel cell degradation under start-stop operating condition. *Applied Energy*, 223, 249–262. https://doi.org/10.1016/j.apenergy.2018.04.049

[11] de Bruijn, F. A., Dam, V. A. T., & Janssen, G. J. M. (2008). Review: Durability and degradation issues of pem fuel cell components. *Fuel Cells*, 8(1), 3–22. https://doi.org/10.1002/fuce.200700053

[12] Haile, S. M. (2003). Fuel cell materials and components☆☆☆the golden jubilee issue—selected topics in materials science and engineering: Past, present and future, edited by s. Suresh. *Acta Materialia*, 51(19), 5981–6000. https://doi.org/10.1016/j.actamat.2003.08.004

[13] Debe, M. K. (2012). Electrocatalyst approaches and challenges for automotive fuel cells. *Nature*, 486(7401), 43–51. https://doi.org/10.1038/nature11115

[14] Chalk, S. G., & Miller, J. F. (2006). Key challenges and recent progress in batteries, fuel cells, and hydrogen storage for clean energy systems. *Journal of Power Sources*, 159(1), 73–80. https://doi.org/10.1016/j.jpowsour.2006.04.058

[15] Gewirth, A. A., & Thorum, M. S. (2010). Electroreduction of dioxygen for fuel-cell applications: Materials and challenges. *Inorganic Chemistry*, 49(8), 3557–3566. https://doi.org/10.1021/ic9022486

[16] Abdul Rasheed, R. K., Liao, Q., Caizhi, Z., & Chan, S. H. (2017). A review on modelling of high temperature proton exchange membrane fuel cells (Ht-pemfcs). *International Journal of Hydrogen Energy*, 42(5), 3142–3165. https://doi.org/10.1016/j.ijhydene.2016.10.078

[17] Shahgaldi, S., & Hamelin, J. (2015). Improved carbon nanostructures as a novel catalyst support in the cathode side of PEMFC: A critical review. *Carbon*, 94, 705–728. https://doi.org/10.1016/j.carbon.2015.07.055

[18] Blal, M., Benatiallah, A., NeÇaibia, A., Lachtar, S., Sahouane, N., & Belasri, A. (2019). Contribution and investigation to compare models parameters of (Pemfc), comprehensives review of fuel cell models and their degradation. *Energy*, 168, 182–199. https://doi.org/10.1016/j.energy.2018.11.095

[19] Xu, J., Lu, S., Chen, X., Wang, J., Zhang, B., Zhang, X., … Ding, S. (2017). A high-performance mesoporous carbon supported nitrogen-doped carbon electrocatalyst for oxygen reduction reaction. *Nanotechnology*, 28(48), 485701. https://doi.org/10.1088/1361-6528/aa9406

[20] Álvarez, G., Alcaide, F., Cabot, P. L., Lázaro, M. J., Pastor, E., & Solla-Gullón, J. (2012). Electrochemical performance of low temperature PEMFC with surface tailored carbon nanofibers as catalyst support. *International Journal of Hydrogen Energy*, 37(1), 393–404. https://doi.org/10.1016/j.ijhydene.2011.09.055

[21] Sharma, S., & Pollet, B. G. (2012). Support materials for PEMFC and DMFC electrocatalysts—A review. *Journal of Power Sources*, 208, 96–119. https://doi.org/10.1016/j.jpowsour.2012.02.011

[22] Wang, X., Li, W., Chen, Z., Waje, M., & Yan, Y. (2006). Durability investigation of carbon nanotube as catalyst support for proton exchange membrane fuel cell. *Journal of Power Sources*, 158(1), 154–159. https://doi.org/10.1016/j.jpowsour.2005.09.039

[23] Fang, B., Chaudhari, N. K., Kim, M.-S., Kim, J. H., & Yu, J.-S. (2009). Homogeneous deposition of platinum nanoparticles on carbon black for proton exchange membrane fuel cell. *Journal of the American Chemical Society*, 131(42), 15330–15338. https://doi.org/10.1021/ja905749e

[24] Zhang, X., Xia, X., Ivanov, I., Huang, X., & Logan, B. E. (2014). Enhanced activated carbon cathode performance for microbial fuel cell by blending carbon black. *Environmental Science & Technology*, 48(3), 2075–2081. https://doi.org/10.1021/es405029y

[25] Imran Jafri, R., Rajalakshmi, N., & Ramaprabhu, S. (2010). Nitrogen doped graphene nanoplatelets as catalyst support for oxygen reduction reaction in proton exchange membrane fuel cell. *Journal of Materials Chemistry*, 20(34), 7114. https://doi.org/10.1039/c0jm00467g

[26] Antolini, E. (2012). Graphene as a new carbon support for low-temperature fuel cell catalysts. *Applied Catalysis B: Environmental*, 123–124, 52–68. https://doi.org/10.1016/j.apcatb.2012.04.022

[27] Xin, Y., Liu, J., Zhou, Y., Liu, W., Gao, J., Xie, Y., … Zou, Z. (2011). Preparation and characterization of Pt supported on graphene with enhanced electrocatalytic activity in fuel cell. *Journal of Power Sources*, 196(3), 1012–1018. https://doi.org/10.1016/j.jpowsour.2010.08.051

[28] Sassin, M. B., Garsany, Y., Atkinson, R. W., Hjelm, R. M. E., & Swider-Lyons, K. E. (2019). Understanding the interplay between cathode catalyst layer porosity and thickness on transport limitations en route to high-performance PEMFCs. *International Journal of Hydrogen Energy*, 44(31), 16944–16955. https://doi.org/10.1016/j.ijhydene.2019.04.194

[29] Ye, L., Gao, Y., Zhu, S., Zheng, J., Li, P., & Zheng, J. P. (2017). A Pt content and pore structure gradient distributed catalyst layer to improve the PEMFC performance. *International Journal of Hydrogen Energy*, 42(10), 7241–7245. https://doi.org/10.1016/j.ijhydene.2016.11.002

[30] Barbosa, R., Escobar, B., Cano, U., Ortegon, J., & Sanchez, V. M. (2016). Multiscale relationship of electronic and ionic conduction efficiency in a PEMFC catalyst layer. *International Journal of Hydrogen Energy*, 41(42), 19399–19407. https://doi.org/10.1016/j.ijhydene.2016.04.071

[31] Ambrosio, E. P., Francia, C., Manzoli, M., Penazzi, N., & Spinelli, P. (2008). Platinum catalyst supported on mesoporous carbon for PEMFC. *International Journal of Hydrogen Energy*, 33(12), 3142–3145. https://doi.org/10.1016/j.ijhydene.2008.03.045

[32] Ouattara-Brigaudet, M., Berthon-Fabry, S., Beauger, C., & Achard, P. (2014). Correlations between the catalytic layer composition, the relative humidity and the performance for PEMFC carbon aerogel based membrane electrode assemblies. *International Journal of Hydrogen Energy*, 39(3), 1420–1429. https://doi.org/10.1016/j.ijhydene.2013.09.107

[33] Dicks, A. L. (2006). The role of carbon in fuel cells. *Journal of Power Sources*, 156(2), 128–141. https://doi.org/10.1016/j.jpowsour.2006.02.054

[34] Gittleman, C., Kongkanand, A., Masten, D., & Gu, W. (2019). Materials research and development priorities for low cost automotive proton-exchange membrane fuel cells. *Current Opinion in Electrochemistry*, S2451910319301565. https://doi.org/10.1016/j.coelec.2019.10.009

[35] Samad, S., Loh, K. S., Wong, W. Y., Lee, T. K., Sunarso, J., Chong, S. T., & Wan Daud, W. R. (2018). Carbon and non-carbon support materials for platinum-based catalysts in fuel cells. *International Journal of Hydrogen Energy*, 43(16), 7823–7854. https://doi.org/10.1016/j.ijhydene.2018.02.154

[36] Job, N., Pereira, M. F. R., Lambert, S., Cabiac, A., Delahay, G., Colomer, J.-F., … Pirard, J.-P. (2006). Highly dispersed platinum catalysts prepared by impregnation of texture-tailored carbon xerogels. *Journal of Catalysis*, 240(2), 160–171. https://doi.org/10.1016/j.jcat.2006.03.016

[37] Vandam, H. (1991). Preparation of platinum on activated carbon. *Journal of Catalysis*, 131(2), 335–349. https://doi.org/10.1016/0021-9517(91)90269-A

[38] Frelink, T., Visscher, W., & van Veen, J. A. R. (1995). Particle size effect of carbon-supported platinum catalysts for the electrooxidation of methanol. *Journal of Electroanalytical Chemistry*, 382(1–2), 65–72. https://doi.org/10.1016/0022-0728(94)03648-M

[39] Cazorla-Amorós, D., Alcañiz-Monge, J., de la Casa-Lillo, M. A., & Linares-Solano, A. (1998). Co_2 as an adsorptive to characterize carbon molecular sieves and activated carbons. *Langmuir*, 14(16), 4589–4596. https://doi.org/10.1021/la980198p

[40] Goettmann, F., Thomas, A., & Antonietti, M. (2007). Metal-free activation of co2 by mesoporous graphitic carbon nitride. *Angewandte Chemie International Edition*, 46(15), 2717–2720. https://doi.org/10.1002/anie.200603478

[41] Rodríguez-Reinoso, F., Molina-Sabio, M., & González, M. T. (1995). The use of steam and CO2 as activating agents in the preparation of activated carbons. *Carbon*, 33(1), 15–23. https://doi.org/10.1016/0008-6223(94)00100-E

[42] Zhang, F., Cheng, S., Pant, D., Bogaert, G. V., & Logan, B. E. (2009). Power generation using an activated carbon and metal mesh cathode in a microbial fuel cell. *Electrochemistry Communications*, 11(11), 2177–2179. https://doi.org/10.1016/j.elecom.2009.09.024

[43] Kim, P., Joo, J. B., Kim, W., Kim, J., Song, I. K., & Yi, J. (2006). NaBH4-assisted ethylene glycol reduction for preparation of carbon-supported Pt catalyst for methanol electro-oxidation. *Journal of Power Sources*, 160(2), 987–990. https://doi.org/10.1016/j.jpowsour.2006.02.050

[44] Mu, S., Xu, C., Gao, Y., Tang, H., & Pan, M. (2010). Accelerated durability tests of catalyst layers with various pore volume for catalyst coated membranes applied in PEM fuel cells. *International Journal of Hydrogen Energy*, 35(7), 2872–2876. https://doi.org/10.1016/j.ijhydene.2009.05.022

[45]1`Corradini, P. G., Pires, F. I., Paganin, V. A., Perez, J., & Antolini, E. (2012). Effect of the relationship between particle size, inter-particle distance, and metal loading of carbon supported fuel cell catalysts on their catalytic activity. *Journal of Nanoparticle Research*, *14*(9). https://doi.org/10.1007/s11051-012-1080-5